Gastro Hep Advances 2022;1:807–823

ORIGINAL RESEARCH—BASIC

Specific Temporal Requirement of Prox1 Activity During Pancreatic Acinar Cell Development

Angelica S. Martinez-Ramirez,[1] Thomas L. Borders,[1] Leena Paul,[2] Matthew Schipma,[3] Xinkun Wang,[3] Farida Korobova,[4] Christopher V. Wright,[5] and Beatriz Sosa-Pineda[1]

[1]Department of Medicine, Feinberg Cardiovascular and Renal Research Institute, Northwestern University Feinberg School of Medicine, Chicago, Illinois; [2]Department of Genetics, St. Jude Children's Research Hospital, Memphis, Tennessee; [3]Center for Genetic Medicine, Northwestern University Feinberg School of Medicine, Chicago, Illinois; [4]Center for Advanced Microscopy, Northwestern University Feinberg School of Medicine, Chicago, Illinois; and [5]Department of Cell and Developmental Biology, Vanderbilt University, Nashville, Tennessee

BACKGROUND AND AIMS: An interactive regulatory network assembled through the induction and downregulation of distinct transcription factors governs acinar cell maturation. Understanding how this network is built is relevant for protocols of directed pancreatic acinar differentiation. The murine transcription factor Prox1 is highly expressed in multipotent pancreatic progenitors and in various mature pancreatic cell types except for acinar cells. In this study, we investigated when is Prox1 expression terminated in developing acinar cells and the potential involvement of its activity in acinar cell specification/differentiation. We also investigated the effects of sustained Prox1 expression in acinar maturation and maintenance. **METHODS:** Prox1 acinar expression was analyzed by immunofluorescence and confocal microscopy. *Prox1*-null embryos ($Prox1^{GFPCre/\Delta}$), $Prox1^{AcOE}$ transgenic mice, histologic and immunostaining methods, transmission electron microscopy, functional assays, and quantitative RNA and RNA-sequencing methods were used to investigate the effects of Prox1 functional deficiency and sustained Prox1 expression in acinar maturation and homeostasis. **RESULTS:** Immunostaining results reveal transient Prox1 expression in newly committed embryonic acinar cells. RNA-sequencing demonstrate precocious expression of multiple "late" acinar genes in the pancreas of $Prox1^{GFPCre/\Delta}$ embryos. $Prox1^{AcOE}$ transgenic mice carrying sustained Prox1 acinar expression have relatively normal pancreas development. In contrast, $Prox1^{AcOE}$ adult mice have severe pancreatic alterations involving reduced acinar gene expression, abnormal acinar secretory granules, acinar atrophy, increased endoplasmic reticulum stress, and mild chronic inflammation. **CONCLUSION:** Prox1 transient expression in early acinar cells is necessary for correct sequential gene expression. Prox1 expression is terminated in developing acinar cells to complete maturation and to preserve homeostasis.

Keywords: Prox1; Acinar Cell; Maturation

Introduction

The exocrine pancreas comprises more than 95% of the organ's mass and consists of acinar cells that produce the zymogens of digestive enzymes and ducts of different calibers that solubilize the secreted zymogens in a bicarbonate fluid and transport the secretions to the duodenum. Pancreatic acinar cells have the greatest rate of protein synthesis of any mammalian organ, and they are uniquely bestowed with abundant endoplasmic reticulum (ER) to support that role.[1,2] In the mature pancreas, acinar cell functions are exclusively dedicated to the synthesis, quality control, transport, packaging, storage, and regulated exocytosis of proteins.[3,4]

In mice, pancreatic acinar cells originate from a multipotent progenitor cell (MPC) population that emerges at the periphery of the epithelial plexus at around embryonic day [E] 11.5 and subsequently segregates to the tips of the branches at around E12.5 to E14.5.[5] MPCs give rise to 2 types of progenies: acinar cell precursors and bipotent precursors that produce ductal and endocrine cell progeny.[4] MPCs are distinguished by the expression of carboxypeptidase A (Cpa) and the transcription factors (TFs) Ptf1a and c-Myc. As MPCs undergo acinar cell specification, they continue to express high levels of Cpa and Ptf1a and lose the expression of c-Myc.[5] Early differentiating acinar cells begin to express amylase and other digestive enzymes at around E13.5, and in the following days, this cell population continues to proliferate and expand. Acinar cell expansion is accompanied by an orderly program of gene expression that prolongs beyond postnatal stages and is governed by an interactive transcriptional regulatory network.[4]

Abbreviations used in this paper: **CPa, carboxypeptidase A; ER, endoplasmic reticulum; FDR, false discovery rate; H&E, hematoxylin and eosin; MPC, multipotent progenitor cell; qRT-PCR, quantitative real-time polymerase chain reaction; RNAseq, RNA sequencing; TFs, transcription factors; UPR, unfolded protein response.**

Most current article

2772-5723
https://doi.org/10.1016/j.gastha.2022.05.013

Acinar cell specification, differentiation, and maintenance are entirely dependent on the activity of a basic helix-loop-helix TF named Ptf1a. In the early embryonic pancreas, Ptf1a associates with another TF (Rbpj) to form a new regulatory complex (PTF1-J) that promotes growth and regulates morphogenesis.[6–8] PTF1-J activity induces an "early" acinar gene program that includes *Rbpjl* and its encoded TF, Rbpjl. The accumulation of Rbpjl gradually replaces Rbpj in a new complex with Ptf1a named PTF1-L, whose activity is necessary to complete acinar cell maturation.[8] In immature acinar cells, PTF1-L promotes a "late" acinar gene program that includes the genes of most secreted digestive enzymes (including all trypsinogens) and genes encoding proteins required for packaging, intracellular transport, exocytosis, and other functions.[8,9] Acinar cell development and maintenance also require the activities of Mist1/Bhlha15 and Lrh1/Nr5a2. In the pancreas, the TF Mist1 controls the expression of proteins involved in regulated exocytosis and various secretory proteins,[10] and the nuclear hormone receptor Nr5a2 cooperates with PTF1-L to regulate acinar gene expression.[11,12]

Acinar cell development also involves the termination of downregulation of TFs which are expressed at high levels in MPCs.[4] As an example, we published that the homeodomain TF Prox1 is highly expressed in MPC in the mouse embryonic pancreas and is undetected in acinar cells in the postnatal murine pancreas.[13,14] We also demonstrated that Prox1 loss-of-function induces premature expression of a few acinar genes (eg, *Amy*) and simultaneously reduces the expression of several endocrine genes (eg, *Neurog3*, *Ins*, *Gcg*, *Nkx6.1*) in the midgestation (E12.5–E13.5) murine pancreas.[13] Those initial results argued that Prox1 activity opposes acinar specification while favoring endocrine specification in MPCs. Alternatively, Prox1 function could delay acinar cell commitment in MPCs to enable the expansion of this progenitor population.[4,13] To better clarify the functional role of Prox1 in pancreatic acinar development, we examined its expression in murine pancreatic tissues dissected at preacinar and postacinar specification stages. We also used bulk RNA sequencing (RNAseq) to compare gene expression profiles between control and *Prox1*-nullizygous pancreatic specimens dissected at the acinar specification/commitment stage. Additionally, we produced a novel transgenic mouse model to investigate if sustained Prox1 expression is permissive or incompatible with acinar cell maturation and/or maintenance. We report that Prox1 is transiently expressed in early acinar cells in the murine embryonic pancreas and reveal a new role of this TF during pancreas development involving the establishment of temporal gene expression in newly specified acinar cells. In addition, we demonstrate that Prox1 activity is incompatible with acinar cell maturation since its persistent expression reduces digestive protein expression, impairs secretory granule formation, increases ER stress, and promotes a pathology reminiscent of mild chronic pancreatitis.

Materials and Methods

Mice

$Prox1^{GFPCre/\Delta}$ mice are described elsewhere.[41] $Prox1^{loxP/+}$ mice are described elsewhere.[42] $Prox1^{GFPCre/\Delta}$ mice were crossed with $Prox1^{loxP/+}$ to generate Prox1-null mice. $Ptf1^{Cre/+}$ mice (expressing Cre recombinase in pancreatic progenitors and pancreatic acinar cells) are described elsewhere.[7] *CAG-loxP-eGFP-STOP-loxP-Prox1-IRES-β-gal* mice are described elsewhere.[15] $Ptf1^{Cre/+}$ mice and *CAG-loxP-eGFP-STOP-loxP-Prox1-IRES-β-gal* mice were crossed to produce $Ptf1a^{Cre/+}$;*CAG-loxP-eGFP-STOP-loxP-Prox1-IRES-β-gal* transgenic progeny (hereafter named $Prox1^{AcOE}$). $Prox1^{GFPCre/\Delta}$ mice and $Prox1^{loxP/+}$ mice were on an Naval Medical Research Institute genetic background. The other mice in the study were on a mixed genetic background. All animal experiments were performed in accordance with protocols reviewed and approved by the Institutional Animal Care and Use Committee at Northwestern University. Mice were treated in accordance with the criteria outlined in the Guide for the Care and Use of Laboratory Animals of the National Institutes of Health.

RNA Isolation and Quantitative PCR

E13.5 and E17.5 pancreatic RNAs were isolated using TRIzol Reagent (Invitrogen, Whaltham, MA, USA) and the RNeasy Plus Micro Kit (50) (Cat.74034; Qiagen, Hilden, Germany). P4, P7, and P30 pancreata were collected in RNAlater (Cat AM7021; Invitrogen, Whaltham, MA, USA), incubated overnight at 4 °C, and frozen at −80 °C before isolating the RNA using TRIzol Reagent and the PureLink RNA Mini Kit (Cat. 12183018A; Invitrogen, Whaltham, MA, USA) following the manufacturer's instructions. The cDNA was synthesized using the iScript Reverse Transcription Supermix for RT-qPCR (Cat 1,708,840; Bio-Rad, Hercules, CA, USA) following the manufacturer's instructions. iTaq Universal SYBR R Green Supermix (Cat. 1725121; Bio-Rad, Hercules, CA, USA) was used for quantitative PCR. qRT-PCR was performed on a Mastercycler Realplex machine (Eppendorf, Hamburg, Germany). Expression levels were determined with gene-specific primers. Data were analyzed with the relative standard curve method and were normalized to *beta-actin* (*ActB*) or *Gapdh* expression. Table A6 lists the primers used for quantitative PCR.

Tissue Processing

Mouse embryos and newborn and postnatal pancreata (up to P21) were dissected and prepared as described in the following text. P30 and older mice were anesthetized with 2, 2, 2-Tribromoethanol (Avertin) (Cat. T48402; Sigma-Aldrich, St Luis, MO, USA) and perfused intracardially with 4% paraformaldehyde before the pancreas was harvested. Tissues or embryos used for cryosectioning were fixed overnight in 4% paraformaldehyde at 4 °C, incubated one more night in 30% sucrose at 4 °C, and embedded in Tissue-Tek OCT Compound, (Cat. 4583; Sakura, Torrance, CA, USA). Pancreata used for paraffin sectioning were fixed overnight in 4%

paraformaldehyde at 4 °C, dehydrated in a graded ethanol series, and embedded in paraffin.

Histology

The paraffin sections (8 μm) were stained with H&E for morphology analysis. The paraffin sections were stained with Sirius red (Direct Red 80, Cat. 365548; Sigma-Aldrich, St. Luis, MO, USA) or Masson's trichrome (Connective Tissue Stain Kit, Cat. ab150686; Abcam, Cambridge, UK,) to visualize collagen fibers, following the manufacturer's instructions. Bright-field pictures were captured using a Zeiss Axioscop 2 Plus microscope and processed with Adobe Photoshop 7.0 (Adobe Systems).

Immunofluorescence and Imaging

Immunostaining of cryosections was performed as previously reported.[43] Briefly, The 10-μm frozen sections were incubated in blocking solution (Cat. 11096176001; Roche, Mannheim, Germany) for 30 minutes. The sections were then incubated overnight with primary antibodies, fluorescent-conjugated secondary antibodies for 2 hours, and 4',6-diamidino-2-phenylindole (Cat. D1306; Applied Biosystems, Waltham, MA, USA) to stain the nuclei. All incubations were at room temperature. Images were acquired with a Zeiss Axioscop 2 fluorescence microscope or with a confocal Leica DM 2500 microscope and processed with Adobe Photoshop CC (Adobe Systems). Table A7 lists the antibodies used for immunofluorescence.

Immunohistochemistry and Imaging

Immunostaining of paraffin sections was performed as previously reported.[43] Briefly, the 8-μm sections were deparaffinized in xylene, rehydrated in ethanol, and incubated with citrate antigen retrieval buffer in a 2100-Retriever (BioVendor Laboratory, Kassel, Germany). After incubation in blocking solution (Cat. 11096176001; Roche, Mannheim, Germany) for 30 minutes, the sections were incubated with primary antibodies overnight and with biotinylated secondary antibodies for 2 hours. The sections were then incubated with ABC reagent (Cat. PK-4000; Vector Laboratories, Burlingame, CA) for 30 min and with DAB solution (Cat. SK-4100; Vector Laboratories, Burlingame, CA) to visualize the immunocomplexes. Finally, the slides were counterstained with 40% Mayer's hematoxylin (Cat. MHS16-500ML; Sigma-Aldrich, St. Luis, MO, USA) before mounting. All incubations were at room temperature. Images were acquired with a Zeiss Axioscop microscope and processed with Adobe Photoshop CC (Adobe Systems). Table A7 lists the antibodies used for immunohistochemistry.

Phalloidin Staining

Rhodamine Phalloidin (Cat. R415; Thermo Fisher Scientific, Whaltham, MA, USA) was used to stain F-actin fibers following the manufacturer's instructions. Briefly, the Rhodamine Phalloidin reagent (5 μL of a 200 U/mL stock solution dissolved in 100 μL 1X phosphate buffered saline) was added to the slides after immunofluorescence staining and incubated for 20 minutes at room temperature. Afterward, the slides were stained with 4',6-diamidino-2-phenylindole (Cat. D1306; Applied biosystems, Foster City, CA, USA).

Transmission Electron Microscopy

P30 pancreatic specimens were fixed in 0.1 M sodium cacodylate buffer pH7.3 containing 2% paraformaldehyde and 2.5% glutaraldehyde and postfixed with 2% osmium tetroxide in unbuffered aqueous solution, rinsed with distilled water, stained with 3% uranyl acetate, rinsed with distilled water, dehydrated in ascending grades of ethanol, transitioned with propylene oxide, and embedded in resin mixture of the EMbed 812 kit (Cat. RT14120; Electron Microscopy Sciences, Hatfield, PA), cured in a 60 °C oven. Samples were sectioned on a Leica Ultracut UC6 Ultramicrotome. The 1-μm-thick sections were collected and stained with Toluidine Blue O, and 70-nm sections were collected on 200-mesh copper grids. Thin sections were stained with uranyl acetate and Reynolds lead citrate. A FEI Tecnai Spirit G2 120kV transmission electron microscope located at the Northwestern Center for Advanced Microscopy was used for imaging.

Morphometric Analyses

To quantify the acinar, beta cell, and ductal cell areas, the entire pancreas was sectioned at 10 μm with a cryostat, and each 10th consecutive section was incubated with antibodies for E-cadherin, amylase, insulin, and Sox9. The E-cadherin$^+$ area was calculated per field using ImageJ 1.37v software (NIH, Bethesda, USA) and used as reference of total parenchyma area. The amylase$^+$, insulin$^+$, and Sox9$^+$ areas were measured in the same corresponding field using ImageJ 1.37v software to calculate the percentage of acinar, beta cell, and ductal areas with respect to the total parenchyma area. To measure the percentage of acinar tissue expressing the *Prox1/β-gal* transgene, the entire pancreas was sectioned at 10 μm with a cryostat, and each 10th consecutive section was incubated with antibodies for β-galactosidase and amylase. The amylase$^+$ and β-gal$^+$ areas were calculated using ImageJ 1.37v software. To quantify the number of apoptotic cells per field, the entire pancreas was sectioned at 10 μm with a cryostat, and each 10th consecutive section was incubated with antibodies for cleaved Caspase-3 (Asp175). The Casp3$^+$ cells were counted in at least 6 different fields per section using ImageJ 1.37v software. To measure acinar cell size, the entire pancreas of 3 *Prox1*^{AcOE} mice was sectioned at 10 μm, and each 10th consecutive section was incubated with antibodies for E-cadherin, β-galactosidase, and amylase (at least 10 sections per pancreas were collected). ImageJ 1.37v software was used to determine the size of individual Ecad$^+$/β-gal$^+$/amy$^+$ and Ecad$^+$/β-gal$^-$/amy$^+$ acinar cells (the E-cadherin signal was used to delimit the cell border). At least 20 cells per field were counted. To measure the size and number of acinar secretory granules, the pancreas of 2 control and 2 *Prox1*^{AcOE} mice was processed using a transmission electron microscope as described previously. At least 3 pictures per specimen with 5 to 10 acinar cells per field were selected, and the secretory granules were measured and counted with ImageJ 1.37v software.

Edema and Fibrosis Scoring

H&E staining and Sirius red staining were performed separately on 8-μm pancreatic sections, and images were acquired and processed as previously described (6 images from 3 slides covering distinct pancreatic areas, per genotype, per age [1 month and 5 months of age], and per condition [H&E or Sirius red staining]). The severity of edema and fibrosis was blindly graded by a semiquantitative assessment as described in the study by Moreno et al.[44] The edema scores are as follows: 0 (absent), 1 (focally increased between lobules), 2 (diffusely increased between lobules), and 3 (acini disrupted and separated). The fibrosis scores are as follows: 0 (absent), 1 (rare or around ductal margins), 2 (in the parenchyma, $<$50% of the lobules), and 3 (in the parenchyma, $>$50% of the lobules).

Immune Infiltrate Quantification

Immunostaining with anti-CD68 antibodies was performed as described previously on 8-μm pancreatic sections (6 images from 3 slides covering distinct pancreatic areas, per genotype, per age [1 month and 5 months of age]). The images were acquired and processed using ImageJ 1.37v software (NIH, Bethesda, USA) to measure the $CD68^{+}$ area and the total pancreas area per field.

Serum Amylase

Mice were fasted overnight and then administered a bolus of cerulein (70μg/Kg, Cat. C9026; Sigma-Aldrich, St Louis, MO, USA). After 1 hour, the mice were anesthetized by isofluorane inhalation, and blood was extracted from the retro-orbital plexus. The blood was allowed to coagulate at room temperature for 30 minutes and centrifuged at 2000 rpm for 15 minutes to separate the serum. Amylase activity was measured using the Magle Life Sciences Phadebas Amylase Test (Cat. MSPP-1301; VWR Avantor, USA), following the manufacturer's instructions. The diluted serum samples were incubated with the substrate for 15 minutes at 37 °C, filtered, and the absorbance at 620 nm was measured using a Gen5 Synergy 2 plate reader (BioTek, Vermont, USA). Amylase activity was calculated interpolating the absorbance values in the standard curve provided by the manufacturer and multiplied by the dilution factor. Amylase activity was expressed as micromoles per second per liter (μmol/s*L).

Trypsin Activity

Mice were euthanized, and the whole pancreas was dissected. Intrapancreatic trypsin activity was measured using the Trypsin Activity Colorimetric Assay kit (Cat. MAK290; Sigma-Aldrich, St Louis, MO, USA) following the manufacturer's instructions. Briefly, each pancreas was homogenized in 4 volumes of trypsin assay buffer, centrifuged, and 50μL of clear supernatant was transferred to a 96-well plate. The samples were incubated with 1μL of chymotrypsin inhibitor (10mM) for 10 minutes at room temperature. Fifty microliters of trypsin substrate diluted 1:25 in assay buffer was added, and the plate was incubated at 25 °C. The change in absorbance (405 nm) was recorded every 15 minutes in a Gen5 Synergy 2 plate reader for 2 hours. Protein concentration was measured by Bicinchoninic acid assay using the Pierce BCA Protein Assay Kit (Cat. 23225;Thermo Fisher Scientific, Waltman, MA, USA) and reading the absorbance at 562 nm in a Gen5 Synergy2 plate reader. Trypsin activity was calculated as indicated by the manufacturer, normalized to the total protein in the assay mix, and expressed as mU/mL/mg.

RNA Sequencing

E13.5 pancreatic RNA was isolated using TRIzol Reagent (Invitrogen, Whaltham, MA) and the RNeasy Plus Micro Kit (50) (Cat. 74034; Qiagen, Hilden, Germany). P7 pancreata were collected in RNAlater (Cat. AM7021; Invitrogen, Whaltham, MA) and incubated overnight at 4 °C before isolating RNA using TRIzol Reagent and the PureLink RNA Mini Kit (Cat. 12183018A; Invitrogen, Whaltham, MA. USA). RNA quality and quantity were measured using the Agilent 2100 Bioanalyzer System (Agilent Technologies). RNA libraries were prepared using the Tru-Seq mRNA-Seq Library Prep and sequenced using an Illumina HiSeq 4000 instrument at the Northwestern University NUSeq Core facility. The cutoff for determining significantly differentially expressed genes was a false discovery rate (FDR)–adjusted P value $<$ .05 using the Benjamini-Hochberg method. Gene set expression analysis bioinformatics tools were used to further compare gene expression profiles between P7 control and $Prox1^{AcOE}$ pancreata. Personnel at the NUSeq Bioinformatics Core performed the analyses of the data sets and assisted the interpretation of the results. RNAseq data have been deposited in Gene Expression Omnibus under accession numbers GSE178173 and GSE178174.

Western Blot Analysis

Pancreatic tissues were isolated, flash-frozen, and powdered in liquid nitrogen. The tissue samples were sonicated for 30 seconds in ice-cold RIPA buffer (Cat No. 89900; ThermoFisher, Waltman, MA) with complete Protease Inhibitor Cocktail tablets (Cat No. 11697498001; Roche, Indianapolis, IN). The lysates were centrifuged at 4 °C for 15 minutes, and protein was quantified by Bicinchoninic acid assay using the Pierce BCA Protein Assay Kit (Cat No. 23225; Thermo Fisher Scientific, Waltman, MA, USA). A total of 30 μg of protein was loaded per lane. Sodium dodecyl sulfate/polyacrylamide gel electrophoresis, protein transfer, and Western blotting were performed using standard techniques. Table A7 lists the antibodies used for Western blot. SuperSignal West Pico Chemiluminescent Substrate Pierce (Cat No. 34580; Thermo Fisher Scientific, Waltman, MA, USA) was used, and images were obtained using the iBright Imaging Systems (Thermo Fisher Scientific, Waltman, MA, USA). Band intensity was quantified using ImageJ 1.37v software (NIH, Bethesda, USA).

Statistics

The data were analyzed using GraphPad Prism software (version 8; GraphPad Software, San Diego, CA). Data are shown as the mean ± standard error of mean. Statistical significance was determined using 2-tailed unpaired Student t test to compare control and Prox1-null or control and $Prox1^{AcOE}$ groups. Levels of significance are $^{*}P < .05$, $^{**}P < .01$, and $^{***}P < .001$, and $P > .05$ is not significant. Each quantitative experiment was repeated at least 3 times. We consider biological replicates as those mice or tissues subjected to the same

experimental test and technical replicates as individual samples or tissues subjected to the same analysis.

Results

Prox1 is Expressed During a Short Time Window in Early Developing Acinar Cells

Prox1 expression fluctuates in all epithelial cell lineages in the mouse embryonic pancreas and becomes restricted to endocrine, ductal, and centroacinar cells (and excluded from acinar cells) in the postnatal murine pancreas.[13,14] Since Prox1 is highly expressed in MPCs,[13] we hypothesized that its expression must be terminated prior or shortly after acinar cell specification. To investigate this notion, we performed immunofluorescence experiments in the pancreas of wild-type mouse embryos dissected at various developmental stages: acinar cell specification/commitment (~E13.5), early acinar cell differentiation (~E15.5), perinatal stage (E18.5), and postnatal stage (P5). This analysis shows moderate-to-high levels of Prox1 expression in newly specified acinar precursors identified with the specific marker Cpa1[5] and located at the periphery of the expanding epithelial plexus (Figure 1A) in E13.5 pancreata. Also, immunofluorescence results show low but persistent expression of Prox1 in early differentiating acinar cells (amylase$^+$) located at the tip of the branching epithelium (Figure 1B) in E15.5 pancreata. In contrast, Prox1 expression is absent in acinar cells and is visible in ductal cells, centroacinar cells, and islet cells, in the pancreas of E18.5 mouse embryos (Figure 1C) and P5 mouse pups (Figure 1D). These results demonstrate that Prox1 expression persists in newly specified/committed acinar cells during a short time window and is terminated in that cell lineage toward the end of gestation.

To investigate if Prox1 transient expression is relevant for acinar cell development, we compared gene expression profiles between wild-type (control) and *Prox1*-nullizygous (*Prox1*$^{GFPCre/\Delta}$) pancreata dissected at E13.5 using bulk RNAseq. In agreement to our previous findings at E12.5,[13] the new RNAseq data reveal reciprocal changes in acinar and endocrine gene expression in the E13.5 *Prox1*-null pancreas. Specifically, lack of *Prox1* function upregulates multiple acinar genes (Table A1), downregulates numerous endocrine genes (Table A2), and reduces the expression of a few hepatic genes (eg, *Afp*, *Alb*) (Table A2), in the E13.5 murine pancreas. To further examine the effects of Prox1 functional deficiency in acinar gene expression, we compared the levels of "early" and "late" acinar transcripts identified in other studies[8,9] between E13.5 control and *Prox1*-null pancreata using quantitative real-time polymerase chain reaction (qRT-PCR). The results of this analysis show slightly increased expression of a few "early" acinar transcripts[8,9] (*Amy2b*, *Cpa1*, and *Pnliprp1*) in the E13.5 *Prox1*-null pancreas, although among those transcripts, only *Cpa1* is significantly changed (Figure 2). In contrast, numerous "late" acinar transcripts[8,9] appear significantly upregulated in E13.5 *Prox1*-null pancreata, including several trypsinogen transcripts (eg, *Prss1, Prss2, Prss3, Try10, Try4, Try12*, and *Ctrl*) and transcripts encoding granule secretory proteins (eg, *Sync* and *Gp2*) (Figure 2). These new results support and expand our previous report of premature expression of 2 "late" acinar genes (*Prss2* and *Try4*) in the pancreas of E12.5 *Prox*1-null embryos.[13] Finally, the combined results from RNAseq and qRT-PCR analyses show that lack of Prox1 function does not affect the expression of transcripts encoding the key regulators of acinar cell specification and differentiation Ptf1a, Rpbjl, and Rbpj [4] in the embryonic pancreas (Figure 2 and Table A1). Therefore, it is probable that Prox1 expression restricts or delays the activity of PTF1-L in newly committed acinar cells, since the "late" acinar transcripts showing upregulation in E13.5 *Prox1*-null pancreata are known targets of the transcriptional complex formed by Ptf1a and Rbpjl.[8]

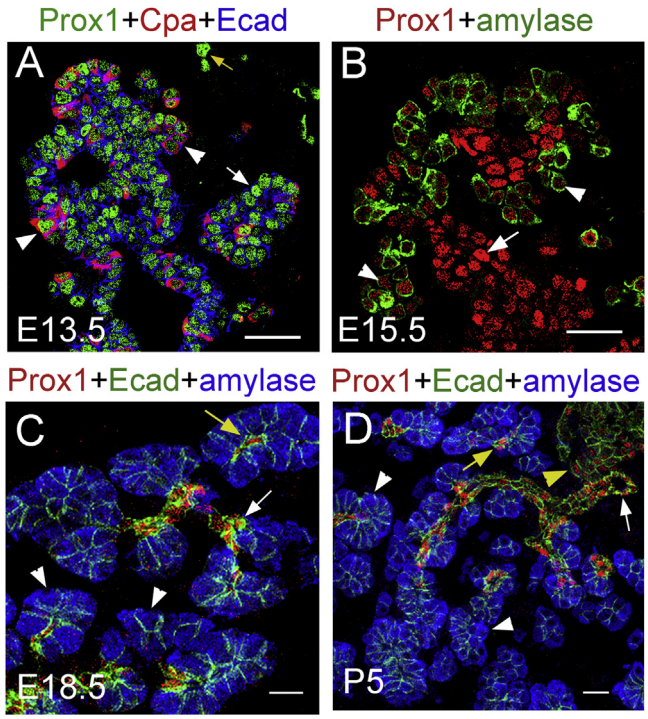

Figure 1. Prox1 is transiently expressed in developing acinar cells. Immunofluorescence images of (A) E13.5, (B) E15.5, (C) E18.5, and (D) P5 wild-type pancreata stained for Prox1 (*green* in A, red in B-D) and co-stained with the acinar markers: carboxypeptidase A1 (*red* in A), amylase (*green* in B and *blue* in C, D), and the epithelial marker E-cadherin (*blue* in A and *green* in C, D). Prox1 is expressed in early developing acinar cells (E13.5, E15.5; *white arrowheads* in A, B) and is absent in perinatal (E18.5; *white arrowheads* in C) and postnatal (P5; *arrowheads* in D) acinar cells. *White arrows* indicate Prox1$^+$ "trunk" cells (A, B) and Prox1$^+$ ductal cells (C, D). *Yellow arrows* indicate Prox1$^+$ lymphatic cells (A) and Prox1$^+$ centroacinar cells (C, D). *Yellow arrowhead* indicates Prox1$^+$ islet cells (D). Images are representative from at least 3 independent experiments. Scale bars = 25 μm.

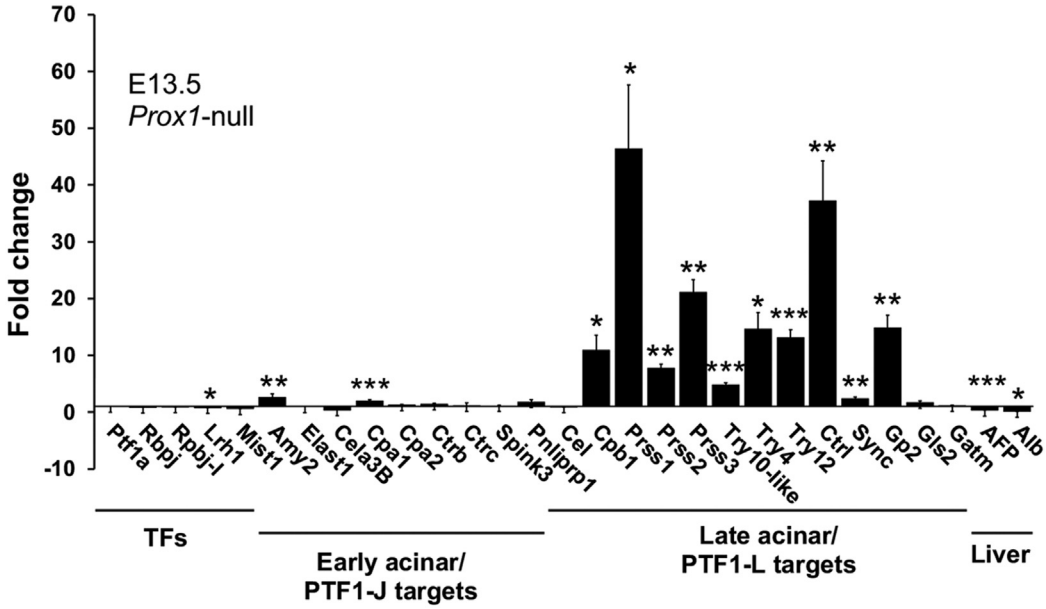

Figure 2. PTF1-L target genes are significantly upregulated in the E13.5 *Prox1*-null pancreas. Expression levels of acinar and liver transcripts in the pancreas of E13.5 *Prox1*-null embryos relative to the expression in E13.5 control pancreas quantified by qRT-PCR. Gene expression was normalized to *Gapdh*. Results are expressed as mean ± SEM (n = 4 samples with 3-4 pancreata per genotype). *$P < .05$; **$P < .01$; ***$P < .001$ by 2-tailed Student *t* test.

Prox1 Continuous Expression Does not Affect Morphogenesis or Suppresses Differentiation in Embryonic Acinar Cells

The rapid extinction of Prox1 expression in embryonic acinar cells raises the possibility that its activity is nonpermissive for acinar cell maturation. To test this hypothesis, we crossed *Ptf1a*$^{Cre/+}$ mice[7] with *CAG-loxP-eGFP-STOP-loxP-Prox1-IRES-β-gal* mice[15] to produce *Ptf1a*$^{Cre/+}$;*CAG-loxP-eGFP-STOP-loxP-Prox1-IRES-β-gal* (or *Prox1*^{AcOE}) transgenic mice carrying sustained Prox1 expression in embryonic, postnatal, and adult pancreatic acinar cells (Figure 3A). Since *Prox1*^{AcOE} mice are heterozygous for *Ptf1a*,[7] all comparisons in our study used pancreatic specimens from *Ptf1a*$^{Cre/+}$ mice as controls (which are not bona fide surrogates of wild-type pancreata). We found that *Prox1*^{AcOE} transgenic mice are viable and look normal at birth, and they survive to adulthood (at least until 5 months of age, which is the end point of the study). The analysis of *Prox1*^{AcOE} embryos dissected at E15.5 using double-immunostaining for β-gal (Figure 3A) and Prox1 demonstrates broad expression of these proteins throughout the pancreas, including the epithelial branching tips where the early developing acinar cells are located (Figure 3B). In contrast, Prox1 levels are low in the epithelial branching tips, and the β-gal reporter is not expressed (Figure 3B) in the pancreas of E15.5 control littermates. Double-immunostaining for amylase and Prox1 in E18.5 and P8 *Prox1*^{AcOE} pancreatic specimens shows broad, moderate Prox1 expression in acinar cells at E18.5 (Figure 3C) and more extensive areas of acinar tissue expressing high levels of Prox1 at P8 (Figure 3D). Conversely, double-immunostaining experiments demonstrate that Prox1 is not expressed in acinar cells in E18.5 and P8 control pancreata (Figure 3C, D). Additional results of hematoxylin and eosin (H&E) staining reveal comparable acinar morphology and overall pancreas architecture between control and *Prox1*^{AcOE} pancreata at E18.5 (Figure 3C) and P8 (Figure 3D). To further examine the *Prox1*^{AcOE} newborn pancreas, we stained this organ from 2 P4 *Prox1*^{AcOE} pups and 2 P4 control littermates with antibodies for the pancreas epithelium marker E-cadherin (Figure 3E), the acinar marker amylase (Figure 3E), the islet marker insulin (Figure 3E), and the ductal marker Sox9 (Figure 3E) and performed morphometric analyses. We found that the overall pancreas size (ie, total E-cadherin$^+$ area) is ∼25% smaller in P4 *Prox1*^{AcOE} mice than in control littermates (Figure 3F). In contrast, the proportion of insulin$^+$ cells, ductal cells, and acinar cells is no different between *Prox1*^{AcOE} pancreata and control pancreata at P4 (Figure 3F). These results demonstrate that while Prox1 continuous expression has no major consequences for fetal acinar morphogenesis or differentiation, it reduces postnatal pancreas growth.

Acinar Cell Morphology is Gradually Disrupted Upon Persistent Prox1 Ectopic Expression

Different to our findings at P8, H&E staining results show focal areas where acinar cells have scarce cytoplasm and enlarged lumens in the pancreas of *Prox1*^{AcOE} mice at preweaning (P15, Figure 4A) and postweaning (P23, Figure 4A) stages. H&E staining also reveals large areas with abnormal acinar tissue, immune cell infiltrates, and conspicuous edema (Figure 4B) in the pancreas of 1-month-old

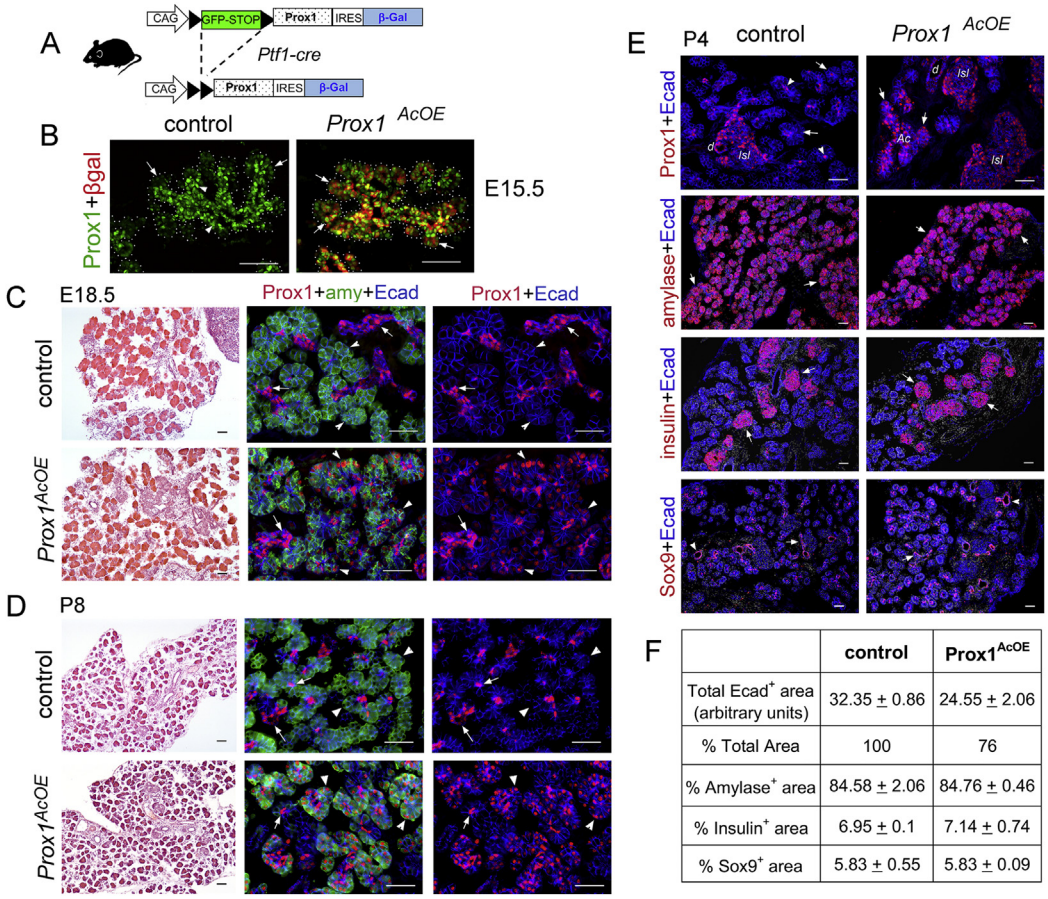

F

	control	Prox1^{AcOE}
Total Ecad$^+$ area (arbitrary units)	32.35 ± 0.86	24.55 ± 2.06
% Total Area	100	76
% Amylase$^+$ area	84.58 ± 2.06	84.76 ± 0.46
% Insulin$^+$ area	6.95 ± 0.1	7.14 ± 0.74
% Sox9$^+$ area	5.83 ± 0.55	5.83 ± 0.09

Figure 3. Persistent expression of Prox1 does not affect fetal acinar cell morphogenesis. (A) Schematic of the *CAG-Prox1-IRES-β-gal* transgene and the production of *Prox1*^{AcOE} (*Ptf1a*$^{Cre/+}$;*CAG-Prox1-IRES-β-gal*) transgenic mice. (B) Immunofluorescence images of E15.5 control (*Ptf1*$^{Cre/+}$) and *Prox1*^{AcOE} pancreata co-stained for Prox1 (*green*) and β-gal (*red*). Prox1 expression (*arrows*) is lower at the branching tips than at the trunk region (*arrowheads*) in the control pancreas. Prox1 and β-gal (*arrows*) are uniformly expressed in the *Prox1*^{AcOE} pancreas. (C, D, *left* panels) H&E staining images show no obvious histologic differences between control and *Prox1*^{AcOE} pancreata at E18.5 (C) and P8 (D). (C, D, *middle* and *right* panels) Immunofluorescence images of E18.5 (C) and P8 (D) pancreata co-stained for Prox1 (*red*), amylase (*green*), and E-cadherin (*blue*). Prox1 is not expressed in acinar cells (*arrowheads*) in the control pancreas at E18.5 (C) and P8 (D). Prox1 acinar expression (*arrowheads*) increases from E18.5 (C) to P8 (D) in the *Prox1*^{AcOE} pancreas. (E, *top*) Immunofluorescence images of P4 pancreata co-stained for Prox1 (*red*) and E-cadherin (*blue*). Prox1 is expressed in ductal (*d*), islet (*isl*), and centroacinar cells (*arrowheads*) in control and *Prox1*^{AcOE} pancreata. Acinar cells (*arrows, Ac*) lack Prox1 expression in control pancreata and show high Prox1 expression in *Prox1*^{AcOE} pancreata. (E) Immunofluorescence images of P4 pancreata co-stained for amylase (*red*) and E-cadherin (*blue*), insulin (*red*) and E-cadherin (*blue*), and Sox9 (*red*) and E-cadherin (*blue*) show similar abundance of acinar tissue (amylase$^+$, *arrows*), beta cells (insulin$^+$, *arrows*), and ductal cells (Sox9$^+$, *arrows*) between control and *Prox1*^{AcOE} pancreata. (F) Quantification of total pancreatic area (Ecad$^+$) and the percentage of acinar (amylase$^+$), beta cell (insulin$^+$), and ductal (Sox9$^+$) areas in P4 control and *Prox1*^{AcOE} pancreata (average ± std. dev. $n = 2$ specimens per genotype). (C, D) The *green* channel is not shown in the images on the right for better comparison of Prox1 expression. Control tissues are *Ptf1*$^{Cre/+}$. Images are representative from at least 3 independent experiments. Scale bars = 50 μm.

Prox1^{AcOE} mice. In contrast, none of the former alterations are noticed in the pancreas of control littermates (Figure 4B). In addition, many acini show abnormal globular shapes and mislocalized nuclei in the pancreas of P30 *Prox1*^{AcOE} mice (Figure 4C), whereas all acini have polygonal-shaped and basolateral-located nuclei in the pancreas of P30 control littermates (Figure 4C). The immunohistochemistry results reveal that the areas of abnormal acinar tissue are infiltrated with macrophages in the pancreas of 1-month-old *Prox1*^{AcOE} mice (Figure 4D). In contrast, only a few resident macrophages are visible in the pancreas of control littermates (Figure 4D). Finally, immunostaining for the apoptosis marker active Caspase-3 shows numerous acinar cells expressing this protein in the pancreas of P30 *Prox1*^{AcOE} mice (Figure 4E), and almost no acinar cells were positive for active Caspase 3 in the pancreas of control littermates (Figure 4E). These results demonstrate that the acinar tissue is gradually lost due to apoptosis and an inflammatory process ensues in the pancreas of *Prox1*^{AcOE} young adult mice.

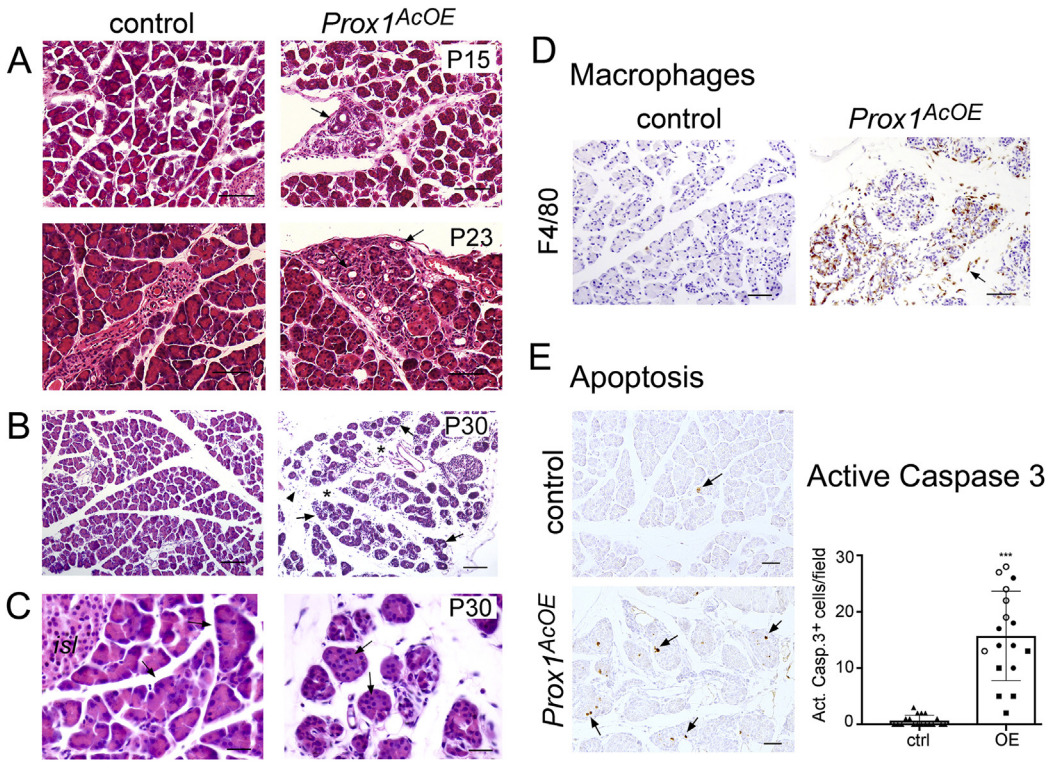

Figure 4. Histologic defects, inflammation, and acinar apoptosis are prevalent in P30 *Prox1*^{AcOE} pancreata. (A) H&E staining images of control and *Prox1*^{AcOE} pancreata dissected at P15 and P23 show focal areas with no acini and aberrant ductal structures (*arrows*) in the *Prox1*^{AcOE} specimens. (B) H&E staining images of P30 control and *Prox1*^{AcOE} pancreata show edema (*asterisks*, *right* panel), immune cells infiltrate (*arrowhead, right* panel), and abnormal acini (*arrows, right* panel) in the *Prox1*^{AcOE} specimen. (C) H&E staining images of P30 control and *Prox1*^{AcOE} pancreata show acini with basolateral nuclei and polygonal shape (*arrows*, *left* panel) in the control specimen, and globular nonpolarized acini (*arrows*, *right* panel) in the *Prox1*^{AcOE} specimen. (D) Immunohistochemistry images of P30 control and *Prox1*^{AcOE} pancreata stained for F4/80 show abundant macrophages (*arrows*) in the *Prox1*^{AcOE} specimen. (E) Immunohistochemistry images of P30 control and *Prox1*^{AcOE} pancreata stained for active Caspase-3 show a single Caspase-3^{+} cell in the control specimen (*arrow*, *left* panel) and numerous Caspase-3^{+} cells in the *Prox1*^{AcOE} specimen (*arrows*, *right* panel). *Right*, Quantification of apoptosis (ie, active Caspase-3^{+} cells per field) in P30 control and *Prox1*^{AcOE} pancreata. Results are expressed as mean ± SEM (n = 6 samples, 3 pancreata per genotype). Symbols correspond to different specimens. ***$P < .001$ by 2-tailed Student *t* test. Control tissues are *Ptf1*$^{Cre/+}$. All images are representative from at least 3 independent experiments. Scale bars = 100 μm (A, *top* panels, B), 50 μm (A, *bottom* panels, D, E), 25 μm (C).

We investigated if the morphologic alterations in *Prox1*^{AcOE} adult pancreata correlate with the extent of Prox1 ectopic acinar expression using immunostaining approaches. This analysis reveals extensive (albeit mosaic) Prox1 expression in the acinar lobules of P30 *Prox1*^{AcOE} pancreata (Figure 5A). In contrast, Prox1 is expressed in islets, ducts, and centroacinar cells but not in acinar cells (Figure 5A) in the pancreas of control littermates. The comparison of Prox1^{+} and Prox1^{-} acini within the same *Prox1*^{AcOE} pancreatic specimen shows that the Prox1^{+} acini are smaller, have less cytoplasm, and their nucleus is mislocalized relative to the adjacent Prox1^{-} acini that have abundant cytoplasm and basolateral nuclei (Figure 5A). Also, double-immunofluorescence experiments to compare β-gal^{+} and β-gal^{-} acini within individual P15 and P30 *Prox1*^{AcOE} pancreatic specimens show normal apical distribution of the protein mucin in acini that do not express β-gal (Figure 5B) and very low or no mucin expression in adjacent β-gal^{+} acini (Figure 5B). Moreover, the results of double-immunofluorescence and morphometric analyses reveal that the average size of β-gal^{+} acinar cells is significantly smaller than the average size of adjacent β-gal^{-} acinar cells (Figure 5C). To quantify the extent of Prox1/β-gal acinar expression in the pancreas of *Prox1*^{AcOE} mice of various ages, we performed double-immunostaining experiments using antibodies for β-gal and amylase. The results show extensive β-gal expression in acinar cells at E18.5 and P7 (Figure 5D) and mosaic expression of β-gal in acinar cells at 1 month and 3 months of age (Figure 5D). Quantification of those results demonstrates that >80% of the *Prox1*^{AcOE} acinar tissue expresses Prox1/β-gal at the perinatal and neonatal stages (Figure 5E), and less than 50% of the *Prox1*^{AcOE} acinar tissue expresses Prox1/β-gal in adult stages (Figure 5E). In conclusion, we discovered that Prox1 persistent expression causes severe morphologic alterations and promotes apoptosis in adult acinar cells. In turn, the lost

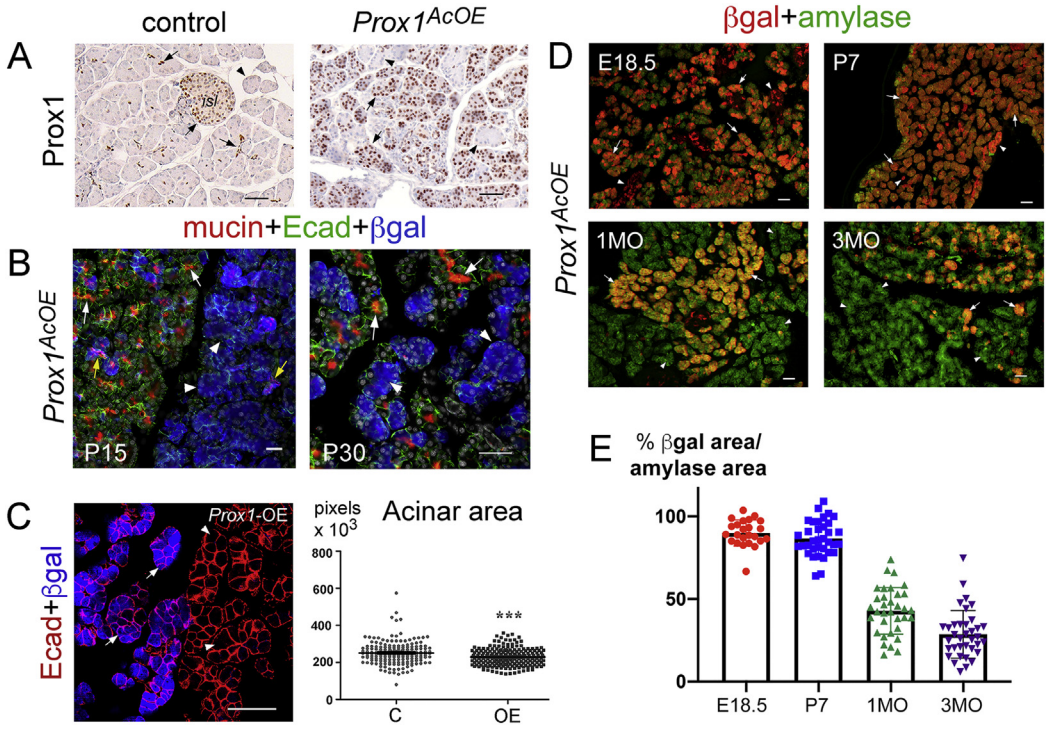

Figure 5. Prox1 ectopic acinar expression is increasingly mosaic in *Prox1*^{AcOE} pancreata. (A) Immunohistochemistry images of P30 control and *Prox1*^{AcOE} pancreata stained for Prox1 show restricted expression in centroacinar, ductal, and islet (*isl*) cells (*arrows*, *left* panel) in the control specimen, and broad mosaic acinar expression in the *Prox1*^{AcOE} specimen (*arrows*, *right* panel; *arrowheads* indicate Prox1^{-} acini). (B) Immunofluorescence images of P15 and P30 *Prox1*^{AcOE} pancreata co-stained for mucin (*red*), E-cadherin (*green*), and β-galactosidase (*blue*) show mucin (*arrows*) expression on the apical side of β-gal^{-} acini and very low or absent mucin expression in β-gal^{+} acini (*arrowheads*; *yellow arrowheads* indicate a few β-gal^{+}/mucin^{+} acini in the P15 specimen). (C, *left*) Confocal immunofluorescence image of P30 *Prox1*^{AcOE} pancreata stained for E-cadherin (*red*) and β-galactosidase (*blue*) shows mosaic expression of β-gal in the acini. The β-gal^{+} acinar cells (*arrows*) look smaller than the β-gal^{-} acinar cells (*arrowheads*). (C, *right*) Results of morphometric analysis show that the median size of the β-gal^{+} acinar cells is smaller than that of the β-gal^{-} acinar cells in P30 *Prox1*^{AcOE} pancreata (n = 3). ***$P < .001$ by 2-tailed Student *t* test. (D) Immunofluorescence images of E18.5, P7, 1- and 3-month-old pancreata co-stained for β-galactosidase (*red*) and amylase (*green*) show increasingly mosaic expression of Prox1/β-gal in the pancreas of *Prox1*^{AcOE} mice from E17.5 to 3 months of age. (E) Quantification of the percentage of β-gal^{+} area in *Prox1*^{AcOE} pancreata of various ages. Results are expressed as mean ± SEM (n = 12 samples, 3 pancreata per genotype). ***$P < .001$ by 2-tailed Student *t* test. Control tissues are *Ptf1*$^{Cre/+}$. All images are representative from at least 2 independent experiments. Scale bars = 50 μm (A, B [*P30*], C, D), 25 μm (B [*P15*]).

acinar tissue is gradually replaced by acinar cells that do not express the Prox1/β-gal transgene.

Prox1^{AcOE} Adult Mice Display Considerable Acinar Atrophy and Features of Mild Chronic Pancreatitis

To investigate the long-term consequence of sustained Prox1 acinar expression, we analyzed the pancreas of 5-month-old *Prox1*^{AcOE} mice by histologic and immunostaining approaches. H&E staining shows portions of relatively intact acinar tissue (Figure 6A) and variable areas with extensive acinar atrophy, edema, lipomatosis, and few normal acini (Figure 6A) in 5-month-old *Prox1*^{AcOE} pancreata. Also, Sirius red and Masson's trichrome staining reveal scattered regions with abundant-to-moderate collagen deposition in those tissues, especially around areas where acinar atrophy is prominent (Figure 6B). The results of immunostaining show that the Prox1^{+} acini are smaller, have unusual globular shape, and lack basolateral nuclear polarity (Figure 6C) in comparison to the surrounding Prox1^{-} acini (Figure 6C). Moreover, the areas showing persistent Prox1 acinar expression appear infiltrated with macrophages (Figure 6C), and the Prox1^{+} acinar cells display very deficient expression of the secretory enzymes amylase and elastase (Figure 6C) in comparison to the adjacent Prox1^{-} acinar cells (Figure 6C). As inflammation, fibrosis and acinar atrophy are features of chronic pancreatitis, we measured several typical pathologic indicators[16] in control and *Prox1*^{AcOE} adult mice. The results of cerulein-induced amylase secretion did not reveal significant differences between control and *Prox1*^{AcOE} mice at 2 months and 5 months of age (Figure 6D). On the other hand, a nonsignificant trend of increased intrapancreatic trypsin activity (Figure 6E) and decreased

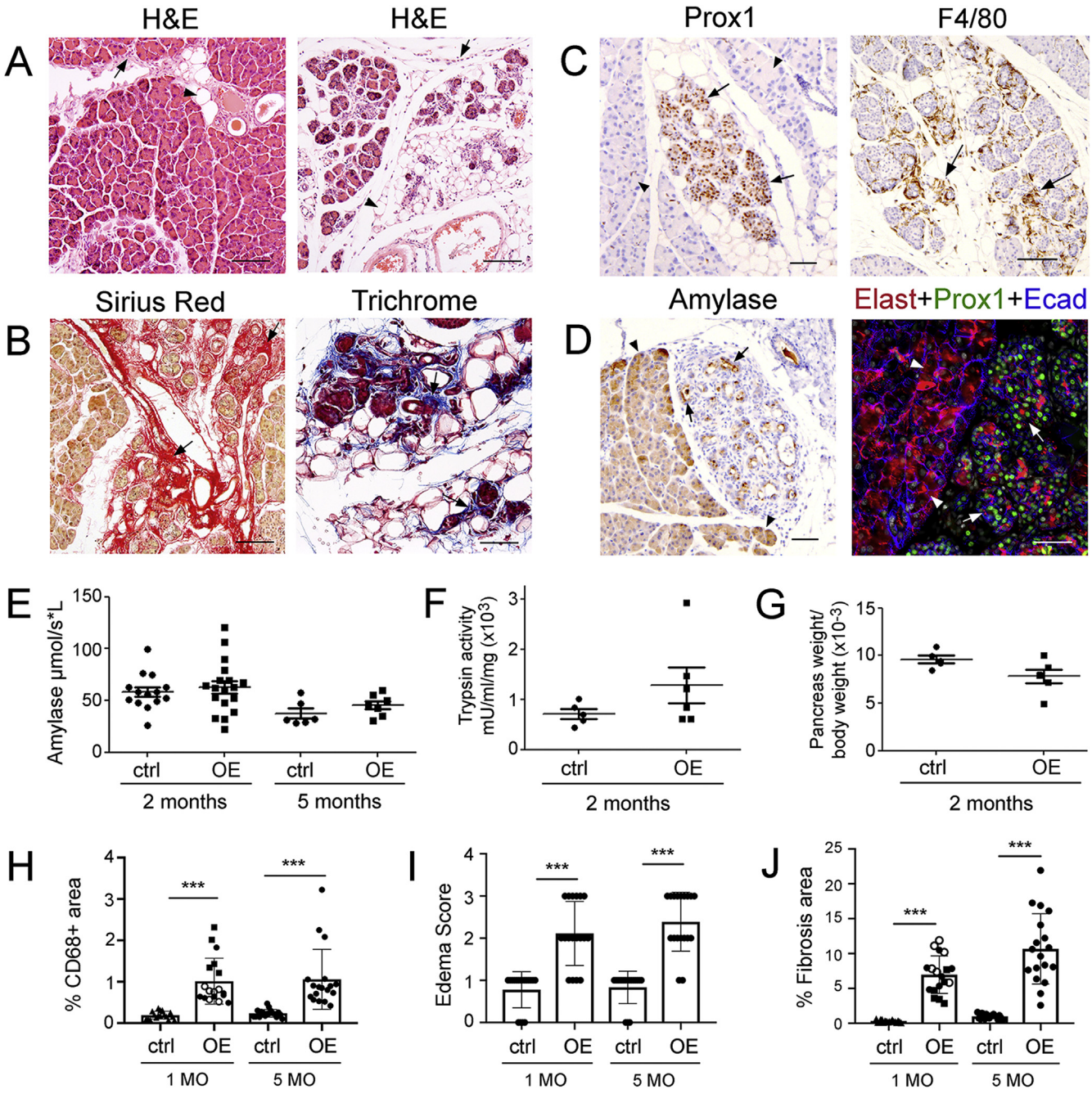

Figure 6. Tissue damage and fibrosis are prevalent in the *Prox1*^{AcOE} adult pancreas. (A) H&E staining images of the 5-month-old *Prox1*^{AcOE} pancreas showing areas with intact acinar tissue (*left*), scarce immune infiltrates (*arrow*, *left*), and lipid deposits (*arrowhead*, *left*) and areas with extensive acinar atrophy (*right*), lipomatosis (*arrowhead*, *right*), and abundant immune infiltrates (*arrows*, *right*). (B) Images of Sirius red (*left*) and mason-trichrome (*right*) staining of the 5-month-old *Prox1*^{AcOE} pancreas showing moderate collagen deposits and fibrosis (*arrows*) in areas with conspicuous acinar atrophy. (C, D) Immunostaining of adjacent sections of a 5-month-old *Prox1*^{AcOE} pancreas shows that the Prox1^{+} acini (C, "Prox1" *arrows*) are smaller and have different morphology compared to the surrounding Prox1^{-} acini; they are infiltrated with macrophages (C, "F4/80" *arrows*) and show very deficient expression of amylase (D, "Amylase" *arrows*) and elastase (D, "Elast" *arrows*). The *arrowheads* indicate normal-looking, Prox1^{-} acini. The immunofluorescence image is stained with elastase (*red*), Prox1 (*green*), and E-cadherin (*blue*). (E) Quantification of serum amylase in 2-month-old (*2 MO*) and 5-month-old (*5 MO*) control (*ctrl*) and *Prox1*^{AcOE} (*OE*) mice (n = 14 [*2 MO*, *ctrl*], 18 [*2 MO*, *OE*], 6 [*5 MO*, *ctrl*], and 7 [5 *MO*, *OE*]). (F) Quantification of intrapancreatic trypsin activity in 2 MO control and *Prox1*^{AcOE} mice (n = 5 *ctrl* and 6 *OE*). (G) Quantification of pancreas weight/body weight in 2 MO control and *Prox1*^{AcOE} mice (n = 4 *ctrl* and 5 *OE*). (H–J) Quantification of macrophage area (H, CD68^{+} cells), edema score (I, H&E staining), and fibrotic area (J, Sirius red staining), in 1-month-old (*1 MO*) and 5-month-old (*5 MO*) control and *Prox1*^{AcOE} mice. Results are expressed as mean ± SEM (n = 6 samples and 3 pancreata per genotype). ***$P < .001$ by 2-tailed Student *t* test. Images are representative from at least 3 independent experiments. Control mice are *Ptf1*$^{Cre/+}$. Scale bars = 100 µm (A, B, C [*Prox1*]), 50 mm (C [*F4/80*] and D).

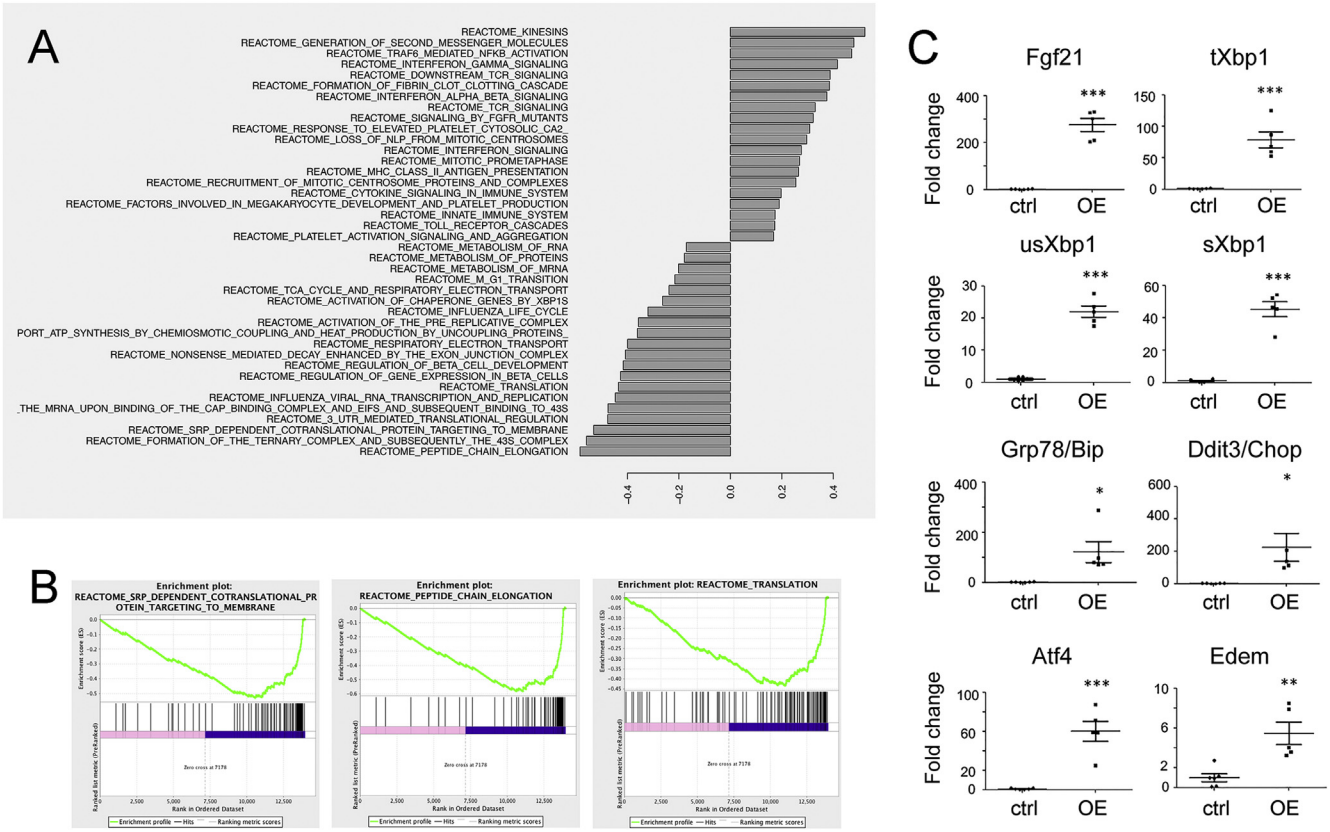

Figure 7. Indicators of ER stress and UPR activation are increased in the pancreas of *Prox1*^{AcOE} mice at P7. (A) Results of gene set enrichment analysis (GSEA) show upregulation of interferon signaling and immune response pathways, and downregulation of pathways involving protein translation, in P7 *Prox1*^{AcOE} pancreata (FDR<0.05). Three independent biological replicates per genotype were used for the RNAseq experiment. (B) GSEA plots show that the most downregulated pathways in P7 *Prox1*^{AcOE} pancreata relate to protein translation. (C) QRT-PCR data showing that markers of ER stress (*Fgf21*) and unfolded protein response (UPR) activation (*tXbp1*, *usXbp1*, *sXbp1*, *Grp78*, *Ddit*, *Atf4*, and *Edem*) are increased in P30 *Prox1*^{AcOE} (OE) pancreata. Gene expression was normalized to *Gapdh*. Control tissues are *Ptf1*$^{Cre/+}$. Results are expressed as mean ± SEM. **P* < .05; ***P* < .01; ****P* < .001 by 2-tailed Student *t* test (n = 6 [control], 5 [*Prox1*^{AcOE}] pancreata). Control tissues are *Ptf1*$^{Cre/+}$.

pancreas weight/body weight (Figure 6F) was uncovered in 3-month-old *Prox1*^{AcOE} mice. Furthermore, significant increases in the abundance of CD68^{+} immune cells (Figure 6G), edema score (Figure 6H), and fibrotic area (Figure 6I) were revealed in the pancreas of *Prox1*^{AcOE} mice at 1 month and 5 months of age. These results demonstrate that sustained Prox1 acinar expression gradually induces a pathologic process recapitulating features of mild chronic pancreatitis.

Bulk RNAseq Reveals Enhanced ER Stress and Activation of the Unfolded Protein Response in Prox1^{AcOE} *Adult Pancreata*

To uncover the underlying mechanisms driving the severe *Prox1*^{AcOE} acinar pathology, we compared gene expression profiles between *Prox1*^{AcOE} and control (*Ptf1*$^{cre/+}$) pancreatic specimens dissected at P7 by bulk RNAseq. This experiment was performed at P7 since no histologic signs of acinar atrophy or conspicuous inflammation were noticed in *Prox1*^{AcOE} pancreata prior to P15 (Figures 3 and 4). Evaluation of the RNAseq results using gene set expression analysis identifies inflammation and fibroblast growth factor signaling amongst the most significantly upregulated pathways in P7 *Prox1*^{AcOE} pancreata (Figure 7A). Also, the gene set expression analysis results show that pathways involving protein translation are significantly downregulated in the transgenic pancreas (Figure 7A and B). The analysis of individual changes in gene expression reveals that ~80 transcripts show significant upregulation (Table A3) in P7 *Prox1*^{AcOE} pancreata. Some transcripts in that list encode proteins induced by ER stress (eg, Fgf21)[17,18] and proteins that mediate unfolded protein response (UPR) activation downstream of ER stress (eg, Eif2ak3/PERK, Atf5, Atf3, Hspa9/mortalin, Reg3b, and Ddit3/CHOP).[19,20] qRT-PCR approaches were used to validate some of the former results, and the results demonstrate persistent upregulation of transcripts encoding markers of ER stress and UPR activation (*Fgf21*, *sXbp1*, *Atf4*, *Grp78/Bip*, *Ddit3/CHOP*, and

Edem)[19,20] in P30 *Prox1*^{AcOE} pancreata (Figure 7C). These findings indicate that sustained Prox1 expression induces apoptosis in acinar cells via increasing ER stress and promoting UPR activation.

Secretory Granule Defects are Prevalent in the *Prox1*^{AcOE} Adult Pancreas

Analysis of the RNAseq data sets identified ~230 transcripts showing significant downregulation in the pancreas of P7 *Prox1*^{AcOE} mice (Table A4). Many of those genes encode acinar digestive enzymes (eg, Pga5, Pnliprp2, Ctrl, Cel, Pla2g1b, Prss53, Prss8, Try10, Cpn1, Pnlip, Try4, Cela3b, and Pnliprp1), acinar secretory granule proteins (eg, Gp2, Zg16, and Sync), regulators of pancreatic fluid secretion (eg, Aqp12), and acinar TFs (eg, Rbpjl, and Xbp1) (Table A4). We were intrigued by the discovery that some of the most downregulated genes in P7 *Prox1*^{AcOE} pancreata encode major acinar secretory granule proteins (Gp2, Zg16, Aqp12, and Sync).[21,22] To follow up and expand those results, the expression of *Gp2, Zg16*, and *Aqp12* was analyzed in *Prox1*^{AcOE} pancreatic specimens dissected at E17.5, P4,

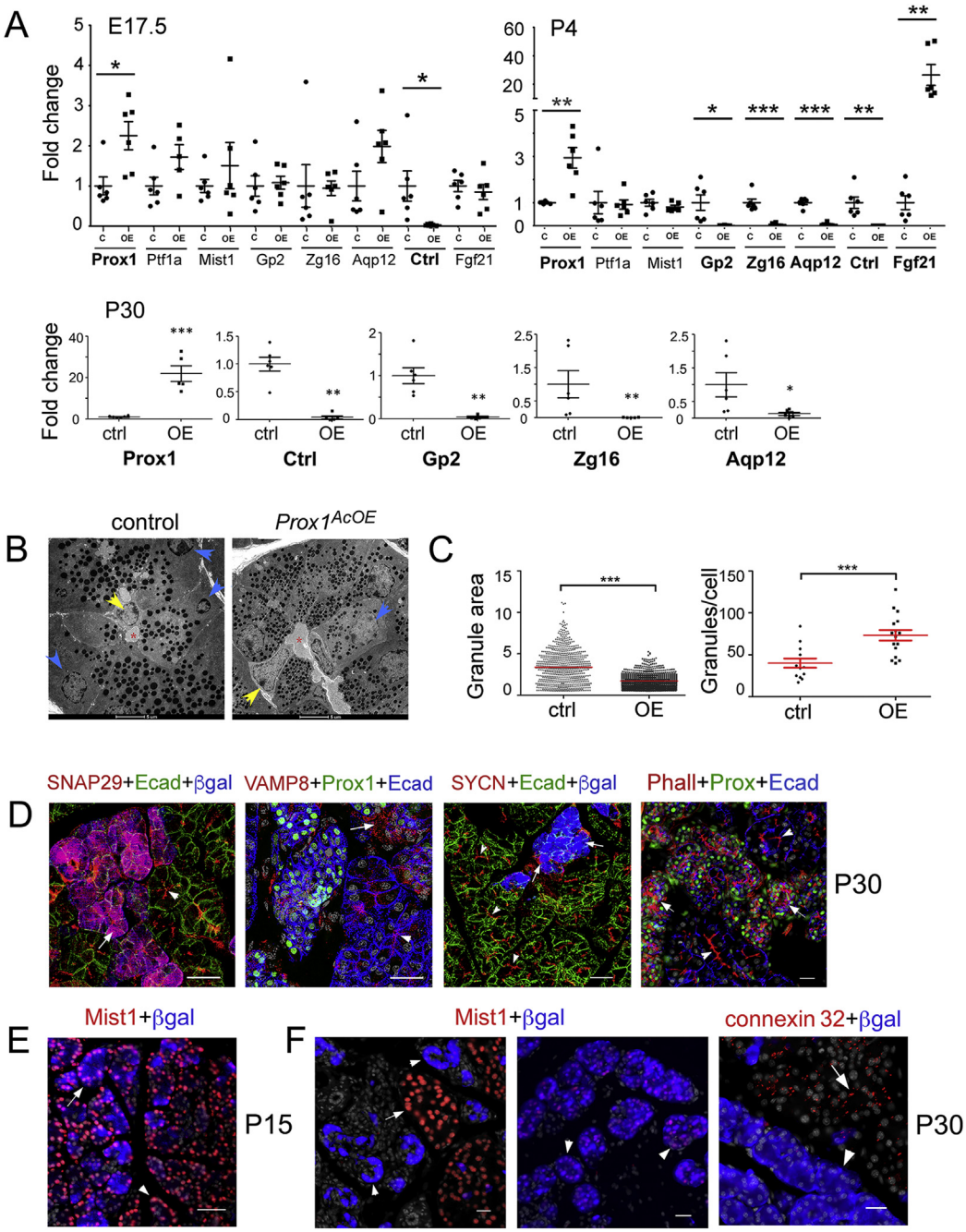

and P30 by qRT-PCR. The results show relatively normal expression of *Gp2*, *Zg16*, and *Aqp12* at E17.5 (Figure 8A) and significant downregulation of those transcripts at P4 and P30 (Figure 8A) in *Prox1*^{AcOE} pancreata. This analysis also demonstrates significantly reduced expression of *Ctrl* from E17.5 onward (Figure 8A) and significant upregulation of the ER stress marker *Fgf21* as early as P4 (Figure 8A) in *Prox1*^{AcOE} pancreata. We also compared the P7 *Prox1*^{AcOE} RNAseq data sets with the E13.5 *Prox1*-nullizygous RNAseq data sets and uncovered opposite changes in the expression of *Ctrl, Sync*, *Prss2*, and *Gp2* in the Prox1 gain-of-function and loss-of-function conditions (Figure A1). These findings suggest that Prox1 activity represses *Ctrl, Sync*, *Prss2*, and *Gp2* in acinar cells.

Since Prox1 ectopic expression downregulates genes that encode major components of acinar secretory granules (eg, *Gp2*,[23,24] *Zg16*,[21] *Aqp12*,[22] and *Sycn*[25]) (Table A3), we analyzed the ultrastructure of those organelles in P30 control and *Prox1*^{AcOE} pancreatic specimens by transmission electron microscopy. This analysis shows large zymogen granules located on the apical side of acinar cells in control pancreata (Figure 8B). In contrast, the zymogen granules look smaller and appear distributed throughout the cytoplasm in acinar cells of *Prox1*^{AcOE} pancreata (Figure 8B). The results of morphometric analysis corroborate that the acinar secretory granules are significantly more numerous and smaller in the pancreas of *Prox1*^{AcOE} mice in comparison to those granules in control pancreata (Figure 8C). We also stained the pancreas of P30 *Prox1*^{AcOE} mice with antibodies for β-gal and various zymogen granule proteins and uncovered marked differences between β-gal^{+} acini and β-gal^{-} acini. Specifically, this analysis reveals normal apical localization of SNAP29 proteins[26] in β-gal^{-} ("normal") acini (Figure 8D) and diffuse cytoplasmic distribution of SNAP29 in β-gal^{+} ("Prox1-positive") acini (Figure 8D). Similarly, VAMP8[26] and syncollin[25] proteins appear concentrated toward the apical side in β-gal^{-} acini (Figure 8D), and they show diffuse and very low expression in β-gal^{+} acini (Figure 8D). We also compared the distribution of F-actin filaments between β-gal^{+} acini and β-gal^{-} acini in the pancreas of P30 *Prox1*^{AcOE} mice. In acinar cells, polymerized F-actin fibers contribute to regulated exocytosis by coating the zymogen granules and stabilizing the fusion of membranes.[27,28] The results of immunofluorescence and phalloidin staining uncovered normal apical distribution of actin filaments (F-actin) in β-gal^{-} acini (Figure 8D) and diffuse mislocalized distribution of F-actin in β-gal^{+} acini (Figure 8D). These collective results demonstrate that Prox1 ectopic expression alters the morphology and localization of secretory granules and disrupts apicobasal polarity in pancreatic acinar cells.

Published studies showed that Mist1 activity establishes and maintains the secretory acinar phenotype in multiple exocrine glands, including the pancreas[29–31]. Since we uncovered a severe secretory granule phenotype in adult pancreatic acinar cells expressing ectopic Prox1, we investigated the expression of Mist1 in *Prox1*^{AcOE} pancreatic specimens dissected at different ages. The results of qRT-PCR analysis and RNA sequencing show comparable *Mist1* transcript expression between control and *Prox1*^{AcOE} pancreata at E17.5, P4, and P7 (Figure 8A and Table A4). Also, the results of double-immunofluorescence analysis using anti-β-gal and anti-Mist1 antibodies show very similar Mist1 expression in β-gal^{-} ("normal") acini and β-gal^{+} ("Prox1-positive") acini (Figure 8E) in the pancreas of P15 *Prox1*^{AcOE} mice. In contrast, the double-immunofluorescence results reveal high Mist1 expression in β-gal^{-}acini (Figure 8F) and very low or no Mist1 expression in β-gal^{+} acini (Figure 8F) in the pancreas of P30 *Prox1*^{AcOE} mice. Western blot results corroborate very reduced expression of Mist1 proteins in the pancreas of P30 *Prox1*^{AcOE} mice (Figure A2).

Figure 8. Secretory granule defects increase with age in *Prox1*^{AcOE}pancreata. (A) *Top*: Expression levels of *Prox1* and the acinar transcripts *Ptf1a*, *Mist1*, *Gp2*, *Zg16*, *Aqp12*, *Ctrl1,* and *Fgf21* in control (*C*) and *Prox1*^{AcOE} (*OE*) pancreata at E17.5 and P4, quantified by qRT-PCR (n = 6 per genotype, per stage). *Bottom*: Expression levels of *Prox1*, *Ctrl*, *Gp2*, *Zg16,* and *Aqp12* in control (*C*) and *Prox1*^{AcOE} (*OE*) pancreata at P30, quantified by qRT-PCR (n = 6 [control] and 5 [*Prox1*^{AcOE}]). Gene expression was normalized to *ActB.* Control tissues are *Ptf1*$^{Cre/+}$. Results are expressed as mean ± SEM. **P* < .05; ***P* < .01; ****P* < .001 by 2-tailed Student *t* test. (B) Transmission electron microscopy images of P30 control and *Prox1*^{AcOE} pancreata show differences in the size, number, and localization of secretory granules. Blue arrows indicate nuclei, yellow arrows indicate centroacinar cells, and red asterisks indicate lumens. (C) Quantification of the number of electron-dense granules per cell (n = 13 cells [control] and 16 cells [*Prox1*^{AcOE}]) and the granule cell area (in pixels^2 x 10^3) (n = 744 granules [control] and 987 granules- [*Prox1*^{AcOE}]). ****P* < .001 by 2-tailed Student *t* test. Three to five separate fields were used for quantification. Control tissues are *Ptf1*$^{Cre/+}$. (D) Immunofluorescence images of the P30 *Prox1*^{AcOE} pancreas stained for the secretory granule proteins SNAP29 (*red*), VAMP8 (*red*), and Syncollin/SYCN (*red*), or for F-actin fibers (with rhodamine phalloidin [*red*]), show very different expression of those proteins in β-gal^{+}/Prox1^{+} (*arrows*) and β-gal^{-}/Prox1^{-} (*arrowheads*) acini. Sections were co-stained for E-cadherin and β-gal or Prox1. Nuclei were stained with DAPI (*gray*). (E) The immunofluorescence image of P15 *Prox1*^{AcOE} pancreata co-stained for Mist-1 and β-galactosidase shows comparable Mist1 expression in β-gal^{+} (*arrow*) and β-gal^{-} (*arrowhead*) acini. (F) *Left and middle*: Immunofluorescence images of P30 *Prox1*^{AcOE} pancreata co-stained for Mist-1 (*red*) and β-galactosidase (*blue*) show high Mist1 expression in β-gal^{-} acini (*arrow*) and very low or no Mist1 expression in β-gal^{+} acini (*arrowheads*). *Right*: The immunofluorescence image of P30 *Prox1*^{AcOE} pancreata co-stained for connexin 32 (*red*) and β-galactosidase (*blue*) shows connexin 32 proteins in β-gal^{-} acini (*arrow*) but not in β-gal^{+} acini (*arrowhead*). Images are representative from at least 2 independent experiments. Scale bars = 5 mm (B), 25 mm (D, F), 50 mm (E).

Additional data from double-immunofluorescence analysis demonstrate expression of the gap junction protein connexin 32 (a known Mist1 pancreatic target[32]) in β-gal$^-$ ("normal") acini (Figure 8G) and lack of connexin 32 expression in β-gal$^+$ ("Prox1-positive") acini (Figure 8G) in the pancreas of P30 *Prox1*^{AcOE} mice. Taken together, our study uncovered a progressive decay in Mist1 protein expression in adult acinar cells expressing ectopic Prox1. Most probably, the lack of Mist1 activity triggered many of the severe secretory granule alterations described earlier and contributed to aggravate the overall *Prox1*^{AcOE} pancreatic pathology.

Discussion

Pancreatic acinar cell maturation is governed by an interactive regulatory network that is gradually assembled through the induction and termination of specific TF functions.[4] In this study, we show that the homeodomain TF Prox1 is transiently expressed in newly committed acinar cells to temporarily arrest the expression of genes encoding secretory digestive zymogens and other "late" acinar proteins.[8,9] We also demonstrate that Prox1 activity is detrimental for acinar cell maturation since its persistent expression downregulates multiple genes encoding secretory enzymes and major zymogen granule proteins, it increases ER stress and induces apoptosis, and it disrupts secretory granule morphology. Furthermore, Prox1 ectopic acinar expression elicits a gradual pathologic process involving inflammation, fibrosis, and other features typical of mild chronic pancreatitis. These new findings demonstrate that Prox1 expression must be tightly regulated during acinar cell development to enable proper maturation and to preserve homeostasis.

The reassessment of E13.5 *Prox1*-nullizygous pancreata by RNAseq analysis uncovered numerous alterations in acinar gene expression that almost certainly involve the activity of PTF1-L. In newly committed acinar cells, PTF1-J and PTF1-L complexes sequentially induce an array of genes encoding digestive enzymes, metabolic proteins, and secretory machinery components.[8,9] At the onset of acinar differentiation (E12.5–E13.5), PTF1-J activates *Cpa1*, *Amy2b*, *Cela*, *Rbpjl*, and a few other "early" acinar genes. Once PTF1-L proteins begin to accumulate (~E15.5), a "late" acinar differentiation program is induced that includes genes encoding digestive proteases (eg, *Prss2*), packaging proteins, secretory proteins, and metabolic regulators.[8] PTF1-L activity also contributes to downregulate *Prox1* in developing acinar cells since Masui et al.[8] reported >3-fold *Prox1* upregulation in the pancreas of E17.5 *Rbpjl*-nullizygous mouse embryos. Using microarray analysis, we previously uncovered ~2-fold increase in *Amy2b* expression and ~48-fold increase in *Prss2* expression in the pancreas of E12.5 *Prox1*-nullizygous embryos.[13] Our new results of RNAseq not only expand the list of acinar genes whose expression is affected by the loss of Prox1 activity in the embryonic pancreas. In addition, those results reveal that the most significantly upregulated acinar genes in the E13.5 Prox1-*Prox1*-null pancreas are targets of PTF1-L, whereas in those mutant tissues, the expression of *Ptf1a, Rbpj*, and *Rbpjl* is not affected. These novel findings and the results in the study by Masui et al.[8] advocate a model whereby Prox1 function restrains PTF1-L activity or prevents PTF1-L formation in early acinar cells. Once the PTF1-L complexes start to accumulate, the expression of Prox1 is terminated, and the "late" acinar gene program is fully activated.

A second prediction of the former model is that sustained Prox1 expression could impair differentiation and/or maturation in acinar cells via antagonizing the activity of PTF1-L. To explore this possibility, we produced *Prox1*^{ACOE} transgenic mice in which Prox1 expression is induced and maintained in the acinar cell lineage. Contrary to our initial hypothesis, the analysis of E17.5 *Prox1*^{ACOE} embryos uncovered minimal effects in acinar cell development under Prox1 continuous expression. However, it is possible that a specific threshold of Prox1 activity is required to affect acinar gene expression since multiple PTF1A target genes showed increased downregulation in the *Prox1*^{ACOE} pancreas between P4 and P7, and we noticed increasing abundance of Prox1 proteins in the *Prox1*^{ACOE} acinar tissue after birth. Many of the PTF1A target genes downregulated in the *Prox1*^{ACOE} postnatal pancreas encode secretory enzymes (*Try10, Try4, Try5*, *Ctrl*, *Prss1*, *Cel*, *Trypsinogen 7*, *Pnliprp1/2*, and *Rnase1*), nonsecretory proteins (*Gatm*, *Gls2*, *Gcat*, *Tmed11*, *Derl3*, *Lfgn*, *Dmbt1*, *Gal*, and *Tff2*), secretory granule proteins (*Gp2*, *Zg16*, *Aqp12*, and *Sync*), regulators of ER protein folding (*Cabp2* and *Erp27*), and acinar TFs (*Rbpjl* and *Spdef*).[8,33] Also, some genes coregulated by PTF1A and MIST1 (*Reg1*)[33] or PTF1-L and NR5A2/LRH-1 (*Ctrl*, *Ela3*, *Klk1*, *Cel*, *Aqp12*, *Gatm*, *Gls2*, *Gal*, and *Chrdl2*)[12] showed downregulation in P7 *Prox1*^{ACOE} pancreata, whereas in those tissues, the expression of *Ptf1a*, *Mist1*, and *Nr5a2* was not affected. Furthermore, although less severe, the *Prox1*^{ACOE} adult acinar phenotype recapitulates many features reported in mice with *Ptf1a* deletion in adult acinar cells, including loss of apicobasal polarity, altered zymogen granule distribution, increased ER stress, apoptosis, and reduced cell size.[33] Therefore, we postulate that Prox1 activity directly or indirectly interferes with the PTF1A regulatory network in immature acinar cells.[33]

Acinar cells have a constitutive UPR to counteract the sustained production of large amounts of unfolded proteins.[1,20,34,35] We uncovered several indicators of enhanced ER stress in the pancreas of *Prox1*^{AcOE} transgenic mice, such as upregulation of *Fgf21* (encoding a protective acinar cell secretagogue induced by ER stress)[17,18] from P4 onward, downregulation of pathways involving protein translation (a major outcome of eIF2α/PERK activation)[20] at P7, upregulation of inflammatory processes (potentially induced by ER stress and the UPR)[36] at P7, and increased expression of canonical indicators of ER stress and UPR activation (eg, *Atf5*, *Eif2ak3*/PERK, *Ddit3*/CHOP, *Hspa9*, *sXbp1*, *Atf4*, *Grp78*/Bip, and *Edem*) [1,17–20] from P7 onward.

Under conditions in which the ER capacity is exceeded, the UPR is activated to inhibit protein synthesis and to promote the degradation of misfolded proteins, and if the damage is excessive or unresolved, the UPR induces cell death.[4,34] Accordingly, the increased acinar cell death that we reported in the pancreas of *Prox1*^{ACOE} mice could be the consequence of activation of the UPR downstream of mounting ER stress. How sustained Prox1 expression increases ER stress in acinar cells is unclear, although this alteration could involve impaired or reduced PTF1A activity[33] since this TF regulates ER homeostasis in acinar cells.[33] Furthermore, we do not rule out that excessive production of Prox1/β-gal proteins contributed to increase ER stress and UPR activation in acinar cells of our *Prox1*^{ACOE} mouse model.

Prox1^{ACOE} adult mice develop a progressive pancreatic pathology involving inflammation, fibrosis, tissue atrophy, and other features reminiscent of chronic pancreatitis. We discovered multiple secretory morphologic alterations involving mislocalized and abnormally small zymogen granules, deficient expression of secretory proteins, aberrant expression of secretory granule proteins implicated in Ca^{2+} regulated exocytosis, a disorganized mesh of F-actin fibers, and loss of apicobasal polarity, in the pancreas of *Prox1*^{ACOE} adult mice. Furthermore, we identified 3 genes encoding essential zymogen granule components (*Gp2*, *Zg16*, and *Aqp12*) amongst the earliest and most downregulated genes in *Prox1*^{ACOE} pancreata. While the former observations suggest that Prox1 activity directly interferes with zymogen granule formation, several results in our study indicate that the loss of Mist1 expression is a major driver of the *Prox1*^{ACOE} adult secretory phenotype. For instance, we found that *Mist1* transcripts and Mist1 proteins have normal expression in *Prox1*^{ACOE} pancreata at P7 to P15, and at those stages, the majority of Prox1/βgal^{+} acinar cells show no obvious morphologic alterations. In contrast, Prox1/βgal^{+} acinar cells show very deficient expression of Mist1 and its target connexin 32 in addition to multiple morphologic secretory alterations in *Prox1*^{ACOE} adult pancreata. The former results argue that as Mist1 expression declines in Prox1^{+} acinar cells, the secretory machinery dismantles, and the pathologic process aggravates. Moreover, it is possible that early-on in the *Prox1*^{ACOE} pathologic process, the expression of Mist1 helps to mitigate a rise in ER stress via inducing the expression of FGF21.[17] Why Mist1 expression lost relatively late in the acinar cells of *Prox1*^{ACOE} mice is unclear, although this alteration could be the result of a specific threshold of Prox1 activity and loss of other acinar TF functions. Interestingly, despite all the previous acinar secretory granule defects, the response to cerulein-induced amylase secretion was relatively normal in *Prox1*^{ACOE} mice. However, we caution that the interpretation of this result is complicated by the fact that all adult transgenic mice retained a sizeable intact acinar mass in their pancreas.

In summary, we uncovered a novel role of Prox1 in newly committed acinar cells involving the temporal regulation of "late" acinar genes (particularly PTF1-L target genes) and demonstrate that sustained Prox1 activity is detrimental for acinar cell maturation and homeostasis possibly through interference with PTF1A functions. The results in our study concur with other publications showing the pathologic effects of sustained or increased expression of TFs that should be downregulated or terminated in acinar cells, such as c-Myc,[37] Pdx1,[38] HNF6/Onecut1,[39] and Sox9.[39,40] Moreover, our findings recommend monitoring the expression of Prox1 in protocols of directed pancreatic acinar differentiation of embryonic or induced-pluripotent stem cells to ensure that proper maturation is achieved.

Supplementary Materials

Material associated with this article can be found in the online version at https://doi.org/10.1016/j.gastha.2022.05.013.

References

1. Pandol SJ. The exocrine pancreas morgan & claypool Life Sciences copyright © 2011. Morgan & Claypool Life Sciences, 2010.
2. Kubisch CH, Logsdon CD. Endoplasmic reticulum stress and the pancreatic acinar cell. Expert Rev Gastroenterol Hepatol 2008;2:249–260.
3. Van Nest GA, MacDonald RJ, Raman RK, et al. Proteins synthesized and secreted during rat pancreatic development. J Cell Biol 1980;86:784–794.
4. MacDonald RJ, Swift GH, Real FX. Transcriptional control of acinar development and homeostasis. Prog Mol Biol Transl Sci 2010;97:1–40.
5. Zhou Q, Law AC, Real FX, et al. A multipotent progenitor domain guides pancreatic organogenesis. Dev Cell 2007;13:103–114.
6. Krapp A, Knöfler M, Ledermann B, et al. The bHLH protein PTF1-p48 is essential for the formation of the exocrine and the correct spatial organization of the endocrine pancreas. Genes Dev 1998;12:3752–3763.
7. Kawaguchi Y, Cooper B, Gannon M, et al. The role of the transcriptional regulator Ptf1a in converting intestinal to pancreatic progenitors. Nat Genet 2002;32:128–134.
8. Masui T, Long Q, Beres TM, et al. Early pancreatic development requires the vertebrate suppressor of hairless (RBPJ) in the PTF1 bHLH complex. Genes Dev 2007;21:2629–2643.
9. Han JH, Rall L, Rutter WJ. Selective expression of rat pancreatic genes during embryonic development. Proc Natl Acad Sci U S A 1986;83:110–114.
10. Pin CL, Rukstalis JM, Johnson C, et al. The bHLH transcription factor Mist1 is required to maintain exocrine pancreas cell organization and acinar cell identity. J Cell Biol 2001;155:519–530.
11. Hale MA, Swift GH, Hoang CQ, et al. The nuclear hormone receptor family member NR5A2 controls aspects of multipotent progenitor cell formation and acinar differentiation during pancreatic organogenesis. Development 2014;141:3123–3133.

12. Holmstrom SR, Deering T, Swift GH, et al. LRH-1 and PTF1-L coregulate an exocrine pancreas-specific transcriptional network for digestive function. Genes Dev 2011;25:1674–1679.
13. Wang J, Kilic G, Aydin M, et al. Prox1 activity controls pancreas morphogenesis and participates in the production of "secondary transition" pancreatic endocrine cells. Dev Biol 2005;286:182–194.
14. Westmoreland JJ, Kilic G, Sartain C, et al. Pancreas-specific deletion of Prox1 affects development and disrupts homeostasis of the exocrine pancreas. Gastroenterology 2012;142:999–1009 e6.
15. Lavado A, Lagutin OV, Chow LM, et al. Prox1 is required for granule cell maturation and intermediate progenitor maintenance during brain neurogenesis. Plos Biol 2010; 8:e1000460.
16. Geisz A, Sahin-Toth M. A preclinical model of chronic pancreatitis driven by trypsinogen autoactivation. Nat Commun 2018;9:5033.
17. Johnson CL, Weston JY, Chadi SA, et al. Fibroblast growth factor 21 reduces the severity of cerulein-induced pancreatitis in mice. Gastroenterology 2009; 137:1795–1804.
18. Coate KC, Hernandez G, Thorne CA, et al. FGF21 is an exocrine pancreas secretagogue. Cell Metab 2017; 25:472–480.
19. Barrera K, Stanek A, Okochi K, et al. Acinar cell injury induced by inadequate unfolded protein response in acute pancreatitis. World J Gastrointest Pathophysiol 2018;9:37–46.
20. Harding HP, Zhang Y, Ron D. Protein translation and folding are coupled by an endoplasmic-reticulum-resident kinase. Nature 1999;397:271–274.
21. Schmidt K, Dartsch H, Linder D, et al. A submembranous matrix of proteoglycans on zymogen granule membranes is involved in granule formation in rat pancreatic acinar cells. J Cell Sci 2000;113(Pt 12):2233–2242.
22. Ohta E, Itoh T, Nemoto T, et al. Pancreas-specific aquaporin 12 null mice showed increased susceptibility to caerulein-induced acute pancreatitis. Am J Physiol Cell Physiol 2009;297:C1368–C1378.
23. Scheele GA, Fukuoka S, Freedman SD. Role of the GP2/THP family of GPI-anchored proteins in membrane trafficking during regulated exocrine secretion. Pancreas 1994;9(2):139–149.
24. Kurashima Y, Kigoshi T, Murasaki S, et al. Pancreatic glycoprotein 2 is a first line of defense for mucosal protection in intestinal inflammation. Nat Commun 2021; 12(1):1067.
25. Wäsle B, Turvey M, Larina O, et al. Syncollin is required for efficient zymogen granule exocytosis. Biochem J 2005;385(Pt 3):721–727.
26. Weng N, Thomas DDH, Groblewski GE. Pancreatic acinar cells express vesicle-associated membrane protein 2- and 8-specific populations of zymogen granules with distinct and overlapping roles in secretion. J Biol Chem 2007;282(13):9635–9645.
27. Valentijn JA, Gien LT, Valentijn KM, et al. An evaluation of the expression, subcellular localization, and function of rab4 in the exocrine pancreas. Biochem Biophys Res Commun 2000;268:847–852.
28. Nemoto T, Kojima T, Oshima A, et al. Stabilization of exocytosis by dynamic F-actin coating of zymogen granules in pancreatic acini. J Biol Chem 2004; 279:37544–37550.
29. Jiang M, Azevedo-Pouly AC, Deering TG, et al. MIST1 and PTF1 Collaborate in Feed-Forward regulatory loops that maintain the pancreatic acinar phenotype in adult mice. Mol Cell Biol 2016;36(23):2945–2955.
30. Hess DA, Strelau KM, Karki A, et al. MIST1 Links secretion and stress as both target and regulator of the unfolded protein response. Mol Cell Biol 2016; 36(23):2931–2944.
31. Lo HG, Jin RU, Sibbel G, et al. A single transcription factor is sufficient to induce and maintain secretory cell architecture. Genes Dev 2017;31(2):154–171.
32. Rukstalis JM, Kowalik A, Zhu L, et al. Exocrine specific expression of Connexin32 is dependent on the basic helix-loop-helix transcription factor Mist1. J Cell Sci 2003;116(Pt 16):3315–3325.
33. Hoang CQ, Hale MA, Azevedo-Pouly AC, et al. Transcriptional maintenance of pancreatic acinar identity, differentiation, and homeostasis by PTF1A. Mol Cell Biol 2016;36:3033–3047.
34. Logsdon CD, Ji B. The role of protein synthesis and digestive enzymes in acinar cell injury. Nat Rev Gastroenterol Hepatol 2013;10:362–370.
35. Harding HP, Zhang Y, Zeng H, et al. An integrated stress response regulates amino acid metabolism and resistance to oxidative stress. Mol Cell 2003;11:619–633.
36. Smith JA. Regulation of cytokine production by the unfolded protein response; implications for infection and autoimmunity. Front Immunol 2018;9:422.
37. Sánchez-Arévalo Lobo VJ, et al. c-Myc downregulation is required for preacinar to acinar maturation and pancreatic homeostasis. Gut 2018;67:707–718.
38. Miyatsuka T, Kaneto H, Shiraiwa T, et al. Persistent expression of PDX-1 in the pancreas causes acinar-to-ductal metaplasia through Stat3 activation. Genes Dev 2006;20:1435–1440.
39. Prevot PP, Simion A, Grimont A, et al. Role of the ductal transcription factors HNF6 and Sox9 in pancreatic acinar-to-ductal metaplasia. Gut 2012;61:1723–1732.
40. Kopp JL, von Figura G, Mayes E, et al. Identification of Sox9-dependent acinar-to-ductal reprogramming as the principal mechanism for initiation of pancreatic ductal adenocarcinoma. Cancer Cell 2012;22:737–750.
41. Srinivasan RS, Geng X, Yang Y, et al. The nuclear hormone receptor Coup-TFII is required for the initiation and early maintenance of Prox1 expression in lymphatic endothelial cells. Genes Dev 2010;24:696–707.
42. Harvey NL, Srinivasa RS, Dillard ME, et al. Lymphatic vascular defects promoted by Prox1 haploinsufficiency cause adult-onset obesity. Nat Genet 2005; 37:1072–1081.
43. Ma R, Martínez-Ramírez AS, Borders TL, et al. Metabolic and non-metabolic liver zonation is established non-synchronously and requires sinusoidal Wnts. Elife 2020; 9:e46206.
44. Moreno C, Nicaise C, Gustot T, et al. Chemokine receptor CCR5 deficiency exacerbates cerulein-induced

acute pancreatitis in mice. Am J Physiol Gastrointest Liver Physiol 2006;291(6):G1089–G1099.

Received July 6, 2021. Accepted May 18, 2022.

Correspondence:
Address correspondence to: Beatriz Sosa-Pineda, PhD, Northwestern University Feinberg School of Medicine, 303 E Superior Street, SQI 8-520, Chicago, Illinois 60611. e-mail: beatriz.sosa-pineda@northwestern.edu.

Acknowledgement:
The authors thank Ming-Yi Chiang and Wanshu Ma (Northwestern University) for technical support, Guillermo Oliver (Northwestern University) for providing the *CAG-Prox1-IRES-LacZ* mice, and the services of the NUSeq Core Facility and the Center for Advanced Microscopy (Northwestern University).

Authors' Contributions:
Beatriz Sosa-Pineda and Angelica S. Martinez-Ramirez conceived, designed, and directed the study and wrote the manuscript. Angelica S. Martinez-Ramirez performed most of the experiments with the assistance of Thomas L. Borders. Leena Paul initiated the study. Xinkun Wang conducted RNA sequencing experiments. Matthew Schipma performed RNA sequencing bioinformatics analysis. Farida Korobova assisted the electron microscopy analysis. Christopher V. Wright provided the *Ptf1*$^{cre/+}$ mice.

Conflicts of Interest:
The authors disclose no conflicts.

Funding:
This study was funded by Northwestern University Feinberg Medical School, National Institutes of Health/National Institute of Diabetes and Digestive and Kidney Diseases grant RO1 DK106266 (BS-P), and Northwestern University's Center for Advanced Microscopy/Cancer Center Support Grant (NCI CA060553).

Ethical Statement:
The corresponding author, on behalf of all authors, jointly and severally, certifies that their institution has approved the protocol for any investigation involving humans or animals and that all experimentation was conducted in conformity with ethical and humane principles of research.

Data Transparency Statement:
Data and analytic methods will be made available to other researchers upon acceptance of the manuscript. Study materials will be available upon request.

GSE178173.
https://www.ncbi.nlm.nih.gov/geo/query/acc.cgi?acc=GSE178173
GSE178174.
https://www.ncbi.nlm.nih.gov/geo/query/acc.cgi?acc=GSE178174